Source parameters and f max in lower Siang region of Arunachal lesser Himalaya

Article *in* Arabian Journal of Geosciences · December 2013

DOI: 10.1007/s12517-013-1223-8

4 authors:

Rohtash Kumar
Banaras Hindu University
26 PUBLICATIONS **706** CITATIONS
SEE PROFILE

S. C. Gupta
Indian Institute of Technology Roorkee
33 PUBLICATIONS **1,500** CITATIONS
SEE PROFILE

Arjun Kumar
Himachal Institute of Engineering & Technology
69 PUBLICATIONS **2,408** CITATIONS
SEE PROFILE

Himanshu Mittal
Ministry of Earth Sciences
71 PUBLICATIONS **1,651** CITATIONS
SEE PROFILE

Arab J Geosci
DOI 10.1007/s12517-013-1223-8

ORIGINAL PAPER

Source parameters and f_{max} in lower Siang region of Arunachal lesser Himalaya

Rohtash Kumar · S. C. Gupta · Arjun Kumar · Himanshu Mittal

Received: 17 July 2013 / Accepted: 26 November 2013

Abstract A data set of 60 local events ($1.9 \leq M_w \leq 3.6$) collected by a temporary digital network deployed in the Siang region of Arunachal Lesser Himalaya during July 2011 to Feburary 2012 is analysed to study the source parameters and f_{max}. The software EQK_SRC_PARA (Kumar et al. in Int J Geosci 3(5):1142–1149, 2012) that considers Brune's model with a high-frequency diminution factor (Boore in Bull Seismol Soc Am 73:1865–1894, 1983) has been used to estimate the spectral parameters namely: low-frequency displacement spectral level (Ω_0), corner frequency (f_c) and f_{max}. These obtained spectral parameters are used to estimate source parameters, namely: seismic moment, source dimension and stress drop and to study the characteristics of f_{max} in this region. Seismic moment varies from 6.13×10^{18} dyn-cm to 3.15×10^{21} dyn-cm; the source radii vary from about 175 to 357 m. The stress drops of these events vary from 0.2 to 56 bars and shows general increasing trend with increase in seismic moment. Various plots of both f_c and f_{max} with seismic moment, focal depth, epicentral distance and site showed the same amount of scatters and trends. From this study, it is found that f_{max} has similar behavior as f_c to seismic moment showing that it is also due to source process, and the same amount of scatter in both cut-off frequencies may be due to either source complexities or site effects or both. Both f_c and f_{max} seems independent of epicentral distance and focal depth. Relationships between f_{max} and seismic moment and stress drop are obtained.

R. Kumar · S. C. Gupta · A. Kumar (✉) · H. Mittal
Department of Earthquake Engineering, Indian Institute of Technology, Roorkee 247667, Uttarakhand, India
e-mail: arjundeq@gmail.com

R. Kumar
e-mail: rohtash21@gmail.com

S. C. Gupta
e-mail: scgupta49@gmail.com

H. Mittal
e-mail: himanshumitt10@gmail.com

Keywords Source parameters · f_{max}, Lower Siang · Arunachal Lesser Himalaya

Introduction

Earthquake source parameters play an important role towards understanding the kinematic and dynamic properties of earthquake source as well as for understanding the seismotectonics of an area and hence for seismic hazard assessment. Earthquake source parameters are generally estimated from the radiated seismic wave-fields. Aki (1967) examined the dependence of the amplitude spectrum of seismic waves on source size on the basis of two dislocation models (ω^3 model and ω^2 model) of an earthquake source. The ω^2 model gives a satisfactory agreement with such observations on the assumption of similarity, but the ω^3 model does not. Brune (1970, 1971) modeled an earthquake source as a tangential stress pulse applied instantaneously to the interior of a dislocation surface. This model employs three independent parameters (moment, source dimension and fractional stress drop) that determine the shape of the far-field displacement spectrum of body waves. He constrained the relationship of the corner frequency to the fault radius by assuming that the effective stress was equal to the average static stress drop.

In the earthquake source models, the acceleration spectrum increases with increasing frequency and become constant beyond corner frequency. Hanks (1982) observed that there is another frequency called the maximum cut-off frequency f_{max} above which acceleration spectral amplitudes diminish abruptly. f_{max} is important from earthquake engineering point of view as it controls the peak ground acceleration. There is a controversy about the origin of this cut-off frequency, f_{max}. However, most of the studies attribute this to the source (e.g. Papageorgiou and Aki 1983a, b; Faccioli 1986; Aki 1987; Papageorgiou 1988; Fujiwara and Irikura 1991; Yokoi and Irikura 1991; Kinoshita 1992; Tsurugi et al. 2000, 2008; Wen

Published online: 12 December 2013

and Chen 2012). Earlier studies by Anderson and Hough (1984) and Anderson (1986, 1991) related this high-cut fall-off to near-surface attenuation, but a recent study by Purvance and Anderson (2003) supports that the high-cut fall-off is primarily controlled by source characteristics as opposed to propagation path effects. Kumar et al. (2013a, b) observed that f_{max} has similar dependence as to f_c for source size, epicentral distance, focal depth and site characteristics. They observed f_{max} seems to be controlled by source process and is independent of epicentral distance and focal depth.

In the present study, source parameters, namely: seismic moment, source dimension and stress drop and another observable spectral parameter f_{max} and its relationship with source, focal depth, epicentral distance and site have been studied using a data set of 60 local events ($1.9 \leq M_w \leq 3.6$) that occurred from July 2011 to February 2012, collected by a temporary digital network deployed in the Siang region of Arunachal Lesser Himalaya.

Seismotectonics of the study area

Among the most dramatic and visible creations of plate–tectonic forces are the lofty Himalayas, which stretch 2,900 km along the border between India and Tibet. This great mountain range began to form between 40 and 50 million years ago, when two large landmasses, India and Eurasia, driven by plate movement, collided. Because both these continental landmasses have about the same rock density, one plate could not be subducted under the other, so this collision creates structural features in the Himalayas. Figure 1 depicts a topographic map along with major tectonic fronts of the Indian Plate on north edge along the Himalayas, i.e. Hazara Arc, Himalayan Arc and Burmese Arc; the area of study (Lower Siang) is also shown by a red box in the map. The Himalayas can be divided structurally (tectonically) from north to south as: Tibetan Himalaya (Northwest part of Arunachal Himalaya bordering Bhutan and Tibet, trending NE–SW), Higher Himalaya (limits between Tibetan Himalaya and MCT, ENE–WSW trend adjacent to Bhutan and changes to NE–SW eastward), Lesser Himalaya (limits between Higher Himalaya and sub-Himalaya, trending E–W in western part, swinging NNE–SSE till the syntaxial then NW–SE), sub-Himalaya (trending E–W near Bhutan, swings ENE–WSW towards east) and the division from east to west: The Eastern Himalaya, Central Himalaya and western Himalaya. (e.g. Gansser 1964; Le Fort 1975).

In the northeastern part of India, is Arunachal Pradesh which mostly occupied by the high mountain range of eastern Himalayas. The Himalayan range enters in Arunachal Pradesh from Bhutan at the west of Kameng district, and the altitude in this region varies from 800–7,000 m above mean sea level. It runs through the northwards region over the Kangto region before ending at the easternmost part of Arunachal Himalaya, i.e. The Namcha Barwa Massif. This part of the Himalayas

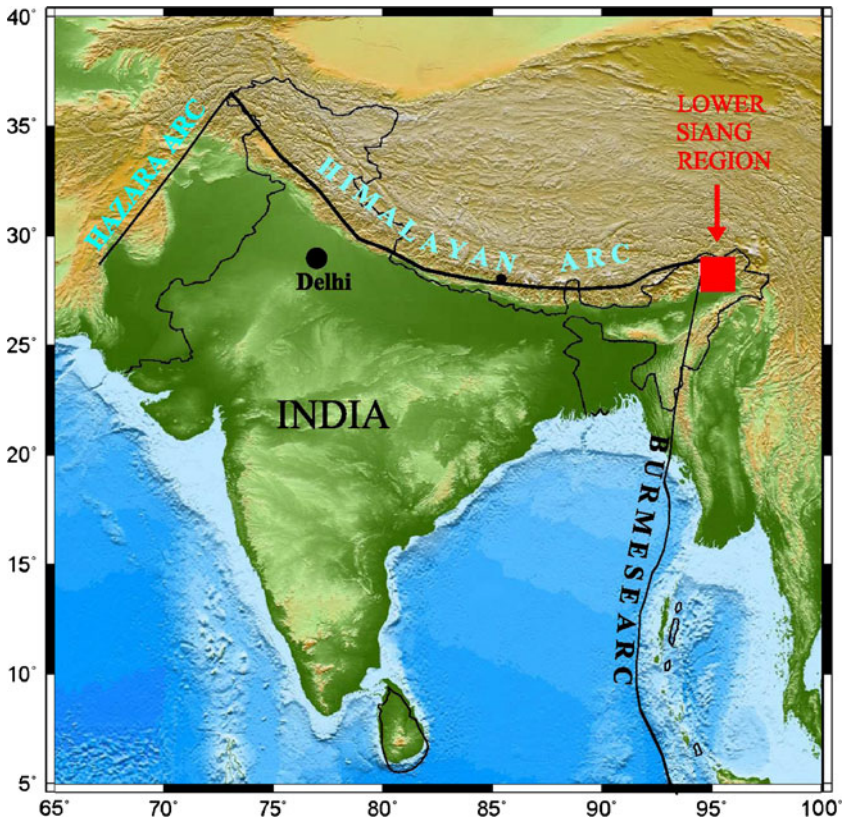

Fig. 1 Map depicts topographic map along with major tectonic fronts of the Indian Plate on north edge along the Himalaya, i.e. Hazara Arc, Himalayan Arc and Burmese Arc. The area of study is also shown as a *red box* in the map

Table 1 Crustal velocity model used for estimation of hypocenter parameters for earthquakes of Siang region of Arunachal Lesser Himalaya

P-wave velocity (km/s)	Depth (km)	Type of rocks	Reference
4.00	0.0	Sedimentary	Khattri et al. 1983 (used in the present study)
6.00	1.0	Granitic	
6.70	25.0	Basaltic	
8.10	45.0	Moho	

includes extensive faulting and over-folding as the major structural element. The regional structural trend of the eastern Himalayas is mostly E–W to ENE–WSW from Bhutan to the northeastern Arunachal Pradesh, which changes gradually to NE–SW near Siang valley and terminates against Siang fracture (e.g. Nandy 1976). Geotechnically, the Arunachal Pradesh can be divided into four geotechnical blocks: the Himalaya, the Mishimi hills, Nagapatkoi ranges of the Arkon Yomo Mountain and Brahmaputra Basin; each of these have experienced intense stages of tectonic development in response to collision of plates and uplift of the Himalayas (Kumar 1997).

From the broad description above, the study region, lower Siang of Siang valley is in Arunachal Himalaya

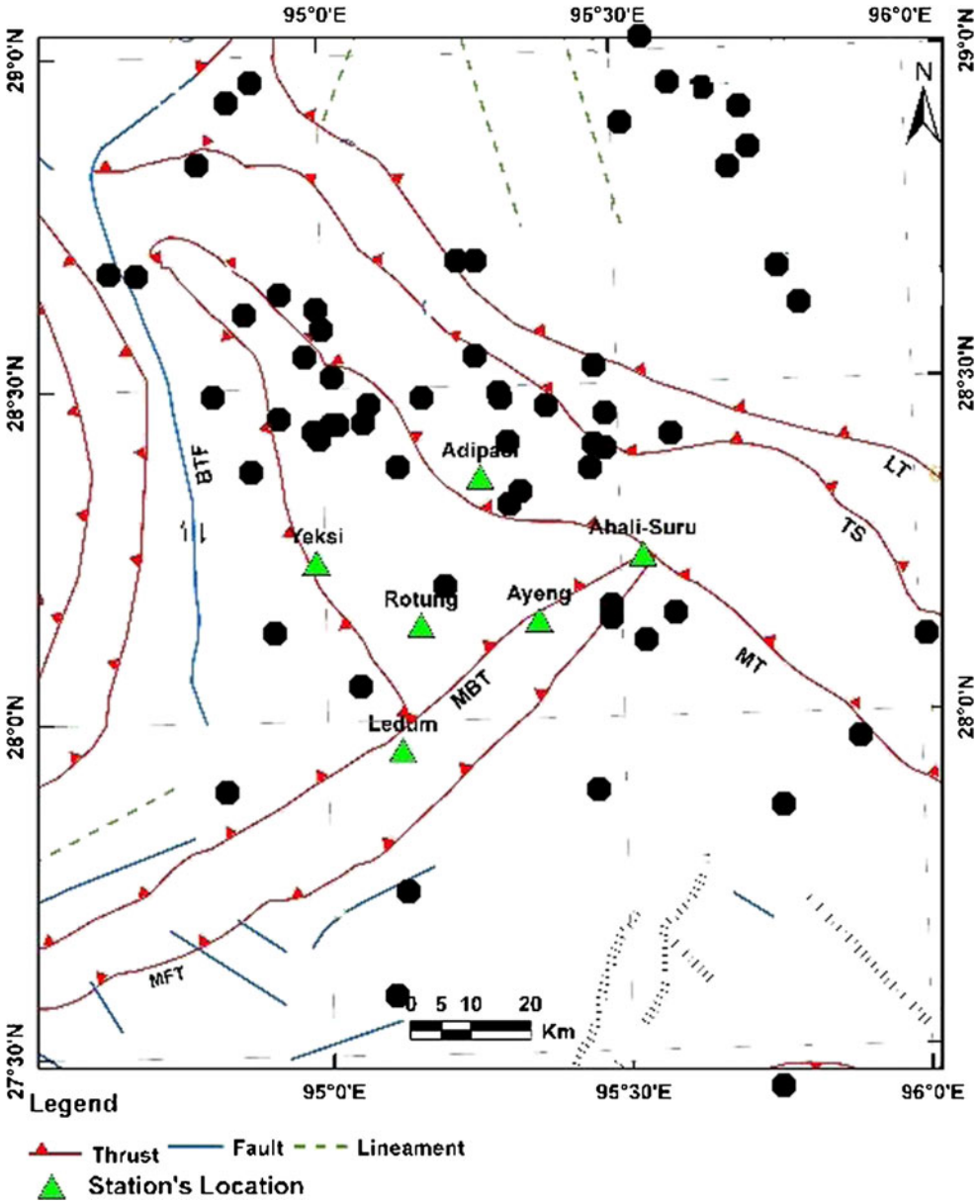

Fig. 2 Map showing epicenters of events recorded during July 2011 to February 2012 (*solid circles*). Tectonics after GSI (2000)

surrounded by Main Frontal Thrust, Main Boundary Thrust in the south, Mishmi Thrust, Tidding Suture and Lohit Thrust in the east and Bame-Tuting Fault in the west. This region is in seismic zone V as per IS Code (IS 1893 (Part 1): 2002) of India. This region shows polyphase deformation, and three stages could be recognised in the region. Six major lithotectonic belts with different litho-stratigraphic settings and deformation patterns separated from one another by regional thrust planes are present in the valley (e.g. Singh and Chowdhary 1990).

Like the other parts of Himalaya, the eastern most Himalaya of Arunachal Pradesh exhibits quiet high seismicity and lies within the seismic zone V as per IS Code (IS 1893 (Part 1): 2002). Several earthquakes of smaller to moderate magnitudes have occurred in this region (Verma et al. 1976; Mukhopadhayay 1984; Kayal 1987). The two great earthquakes namely Shillong (1897) and Assam (1950) earthquakes having magnitudes 8.1 and 8.6, respectively, fell in close proximity to the study region. Shillong earthquake on June 12, 1897 (M_w, −8.1) located near the northern edge of Shillong Plateau while Assam earthquake on August 15, 1950, located in Mishmi hills. On September 18, 2011, the Sikkim earthquake of magnitude M_w 6.9 occurred in proximity to study region.

Data used in the study

A six-station network has been deployed in the lower Siang region of Siang valley for collecting the local earthquake data to examine the seismicity of the region. Three types of sensors have been used for carrying out the study: short-period seismometer, broad band seismometer and an accelerometer. Out of six stations, five are short-period seismometers CMG-40 T1 (Guralp Systems Limited, UK) with sampling rate 100 sps; one is a broad band seismometer CMG-40 T (Guralp Systems Limited, UK) with sampling rate 100 sps; at one station a short-period seismometer has been deployed, an accelerometer CMG-5TC (Guralp Systems Limited, UK) with the purpose of comparing results with seismometer. Each digital seismograph comprised of a 24-bit portable data acquisition system (DL-24) coupled to sensors. A Global Positioning System was used to synchronise data samples to UTC or IST. The local earthquake data collected from digital seismographs during July 2011 to February 2012 have been used in this study.

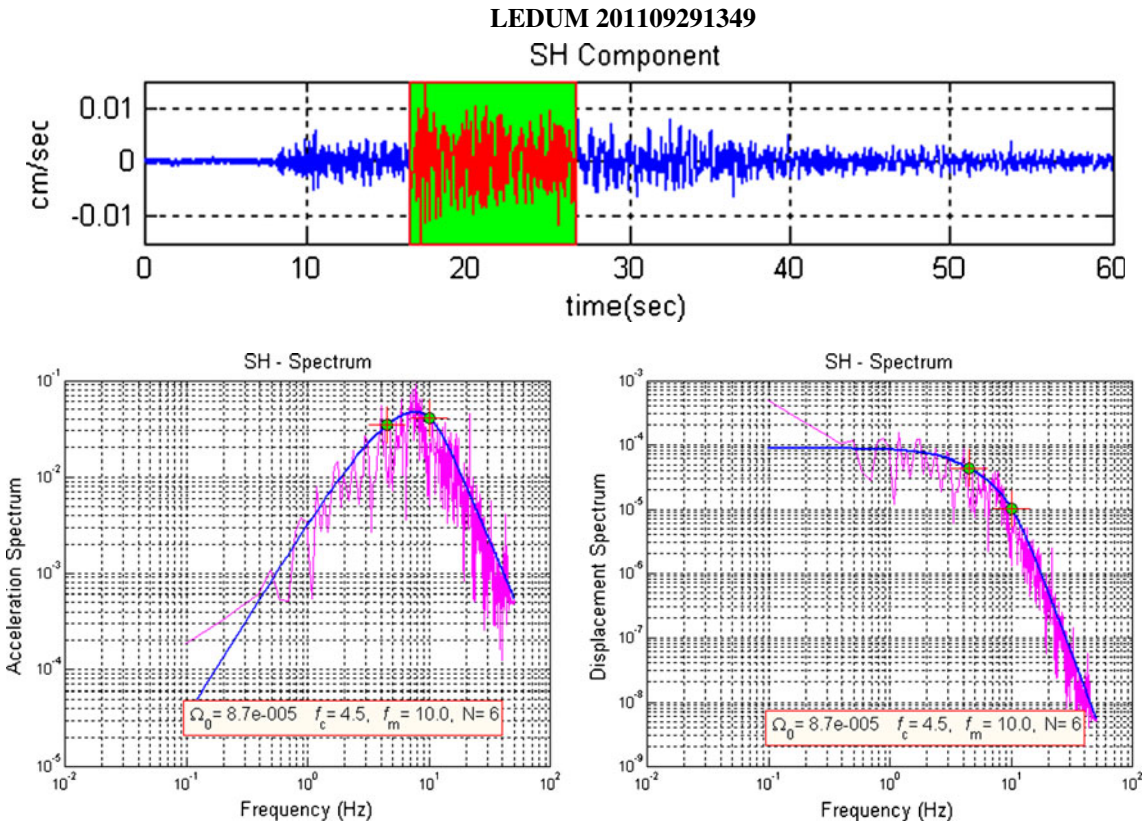

Fig. 3 An example of SH component of time history of earthquake recorded at Lendum on short-period seismograph (*top*). The acceleration (*bottom left*) and displacement (*bottom right*) spectra along with fitted source model

Table 2 Hypocenter parameters and source parameters of earthquakes of Siang region of Arunachal Lesser Himalaya

S. no	Date (yy/mm/dd)	Lat (°E)	Long (°N)	Depth (km)	f_c (Hz)	cp_{max} (Hz)	M_0 (dyn-cm)	Mag. M_w	r (m)	$\Delta\sigma$ (bars)
1.	20/11/07–24	28.83	95.68	8.1	5.1	12.4	5.72×10^{19}	2.5	219.4	2.4
2.	20/11/07–29	28.94	95.57	6.7	5.1	11.0	3.71×10^{20}	3.0	231.1	17.3
3.	20/11/07–29	28.13	94.91	27.6	5.3	11.6	1.75×10^{20}	2.8	210.1	8.2
4.	20/11/07–31	28.94	95.71	6.0	5.0	11.2	2.22×10^{20}	2.9	223.1	8.7
5.	20/11/08–02	28.20	95.20	8.5	5.0	12.2	1.62×10^{19}	2.1	224.9	0.6
6.	20/11/08–05	28.48	95.29	11.26	4.1	10.6	3.77×10^{20}	3.1	275.1	8.0
7.	20/11/08–08	28.73	95.79	39.6	5.3	13.4	1.07×10^{20}	2.7	213.5	4.7
8.	20/11/08–09	28.67	95.81	11.1	3.6	10.5	1.13×10^{20}	2.7	310.6	1.6
9.	20/11/08–09	27.94	94.82	14.1	5.6	15.3	9.46×10^{19}	2.5	232.8	2.8
10.	20/11/08–10	28.42	94.99	23.3	4.5	11.8	1.56×10^{20}	2.8	251.6	4.3
11.	20/11/08–13	28.66	94.63	7.23	4.0	10.4	6.07×10^{20}	3.2	278.4	12.2
12.	20/11/08–15	28.36	95.20	6.34	4.3	11.4	8.31×10^{19}	2.6	258.7	2.1
13.	20/11/08–18	28.66	94.68	6.91	3.8	8.8	2.92×10^{21}	3.6	298.1	48.6
14.	20/11/08–20	28.52	95.24	13.6	4.6	11.4	7.22×10^{19}	2.6	244.5	2.2
15.	20/11/08–30	28.44	95.45	30.98	6.4	12.5	1.38×10^{19}	2.1	174.7	1.1
16.	20/11/09–03	28.48	96.61	35.5	4.1	12.2	2.52×10^{20}	2.9	271.6	5.5
17.	20/11/09–06	28.45	94.92	13.19	3.7	10.4	3.23×10^{20}	3.0	302.0	5.1
18.	20/11/09–08	29.01	95.53	30.72	5.2	10.2	8.34×10^{19}	2.6	214.9	3.7
19.	20/11/09–11	28.37	94.86	14.5	4.4	10.8	2.49×10^{19}	2.3	252.4	0.7
20.	20/11/09–12	28.44	94.98	34.9	3.5	8.6	5.33×10^{20}	3.1	317.7	7.2
21.	20/11/09–14	28.44	95.06	23.68	3.3	10.7	2.60×10^{20}	2.9	342.8	2.8
22.	20/11/09–18	28.54	94.96	6.39	3.3	9.3	4.98×10^{20}	3.1	342.4	5.4
23.	20/11/09–22	28.35	95.31	14.4	5.2	11.5	3.05×10^{20}	3.0	215.9	13.3
24.	20/11/09–26	28.36	95.31	9.38	5.6	11.9	1.24×10^{20}	2.7	201.6	6.6
25.	20/11/09–29	28.44	95.40	12.4	4.4	10.4	4.76×10^{20}	3.1	256.0	12.4
26.	20/11/10–01	28.49	95.29	10.48	5.3	14.1	3.10×10^{19}	2.3	211.2	1.5
27.	20/11/10–05	28.51	95.01	12.85	3.7	9.1	8.25×10^{20}	3.3	299.3	13.4
28.	20/11/10–08	28.44	95.00.	34.4	5.4	17.3	1.28×10^{19}	2.1	208.9	0.6
29.	20/11/10–15	28.34	95.37	8.32	4.0	11.6	9.90×10^{19}	2.7	279.8	2.0
30.	20/11/10–16	28.68	95.22	11.02	5.2	13.2	1.24×10^{19}	2.1	217.0	0.5
31.	20/11/10–17	28.47	95.01	36.5	4.1	16.5	1.36×10^{19}	2.1	273.0	0.3
32.	20/11/10–18	28.47	95.37	11.91	5.0	15.4	1.15×10^{19}	2.0	223.4	0.5
33.	20/11/10–21	29.17	94.82	9.41	4.2	10.2	4.9310^{20}	3.1	266.6	11.3
34.	20/11/11–07	28.46	95.47	12.94	6.1	10.4	8.29×10^{19}	2.6	184.9	5.7
35.	20/11/11–09	28.17	95.59	16.93	4.9	12.0	5.05×10^{19}	2.5	229.8	1.8
36.	20/11/11–10	28.14	96.01	17.55	5.0	12.2	4.80×10^{19}	2.5	224.7	1.9
37.	20/11/11–14	28.60	94.86	11.01	5.1	10.5	1.2810^{20}	3.4	220.2	52.1
38.	20/11/11–15	28.17	95.59	16.76	5.3	13.6	1.19×10^{19}	2.0	212.8	0.5
39.	20/11/11–16	28.70	95.22	10.0	4.1	12.7	1.0910^{21}	3.1	283.0	22.4
40.	20/11/11–18	28.13	95.54	36.12	5.1	10.6	5.18×10^{19}	2.5	220.1	2.1
41.	20/11/11–21	27.61	95.12	11.9	5.5	11.9	2.63×10^{19}	2.3	202.3	1.4
42.	20/11/11–23	28.53	95.45	14.99	5.4	15.3	3.18×10^{19}	2.3	206.5	1.6
43.	20/11/11–23	28.11	95.51	33.08	5.2	15.2	1.31×10^{19}	2.1	215.5	0.6
44.	20/11/12–03	27.86	94.86	17.59	5.3	13.6	1.03×10^{19}	2.0	212.4	0.5
45.	20/11/12–07	28.48	94.78	12.19	4.7	10.8	7.50×10^{19}	2.6	236.3	2.5
46.	20/11/12–09	28.94	94.87	8.0	3.9	10.9	3.15×10^{21}	3.4	291.1	55.5
47.	20/11/12–14	28.18	95.48	19.57	5.0	10.5	2.48×10^{20}	2.9	225.5	9.4
48.	20111216	28.63	94.92	17.11	4.3	10.8	3.78×10^{19}	2.4	263.4	0.9
49.	20/11/12–18	28.58	94.99	9.56	4.7	12.0	1.70×10^{20}	2.8	237.2	5.5

Table 2 (continued)

S. no	Date (yy/mm/dd)	Lat (°E)	Long (°N)	Depth (km)	f_c (Hz)	cp_{max} (Hz)	M_0 (dyn-cm)	Mag. M_w	r (m)	$\Delta\sigma$ (bars)
50.	20/11/12–18	28.06	95.06	11.49	3.2	14.2	2.58×10^{19}	2.3	356.8	0.2
51.	20/11/12–27	27.76	95.14	42.47	4.1	12.5	1.31×10^{20}	2.7	273.2	2.8
52.	20/12/01–01	28.48	94.81	13.14	4.5	13.4	5.04×10^{19}	2.5	251.2	1.4
53.	20/12/01–05	28.47	95.07	30.74	5.4	14.1	6.13×10^{18}	1.9	208.4	0.3
54.	20/12/01–15	27.89	95.77	37.82	4.5	11.7	5.70×10^{19}	2.5	247.6	1.6
55.	20/12/01–30	28.41	95.47	1.53	4.6	14.2	1.64×10^{20}	2.8	246.2	4.8
56.	20/12/02–01	28.48	96.61	35.5	4.6	11.1	7.46×10^{20}	3.2	243.8	22.4
57.	20/12/02–01	28.91	94.98	10.01	3.3	9.7	4.90×10^{20}	3.1	339.6	5.5
58.	20/12/02–13	28.38	95.12	35.35	4.2	10.3	1.92×10^{21}	3.5	269.3	43.0
59.	20/12/02–24	28.68	95.25	10.21	5.4	13.7	2.20×10^{19}	2.2	206.3	1.1
60.	20/12/02–28	28.61	94.98	12.44	4.5	13.0	2.26×10^{19}	2.2	248.5	0.7

Methodology

The time histories are first rotated to obtain SH-component of ground motion, and then spectrum is corrected for instrument response and attenuation due to path. In this study, Brune's model that yields a fall-off of 2 beyond corner frequency is considered with high-frequency diminution factor; a Butterworth high-cut filter presented by Boore (1983) that fits well for frequencies greater than f_{max} is fitted in observed acceleration spectrum as

$$A(R,f) = \frac{(2\pi f)^2 \Omega_0}{\left[1+(f/f_c)^2\right]\left[1+(f/f_{max})^N\right]^{1/2}} \quad (1)$$

And for displacement spectrum

$$D(R,f) = \frac{\Omega_0}{\left[1+(f/f_c)^2\right]\left[1+(f/f_{max})^N\right]^{1/2}} \quad (2)$$

Computer software EQK_SRC_PARA (Kumar et al. 2012) has been used for analysis using the above source model and estimates the spectral parameters, viz. low-frequency displacement spectral level (Ω_0), corner frequency (f_c) and high-cut frequency (f_{max}). The average values of the spectral parameters from different sites have been used to estimate the earthquake source parameters namely seismic moment (M_0), source radius (r) and stress drop ($\Delta\sigma$).

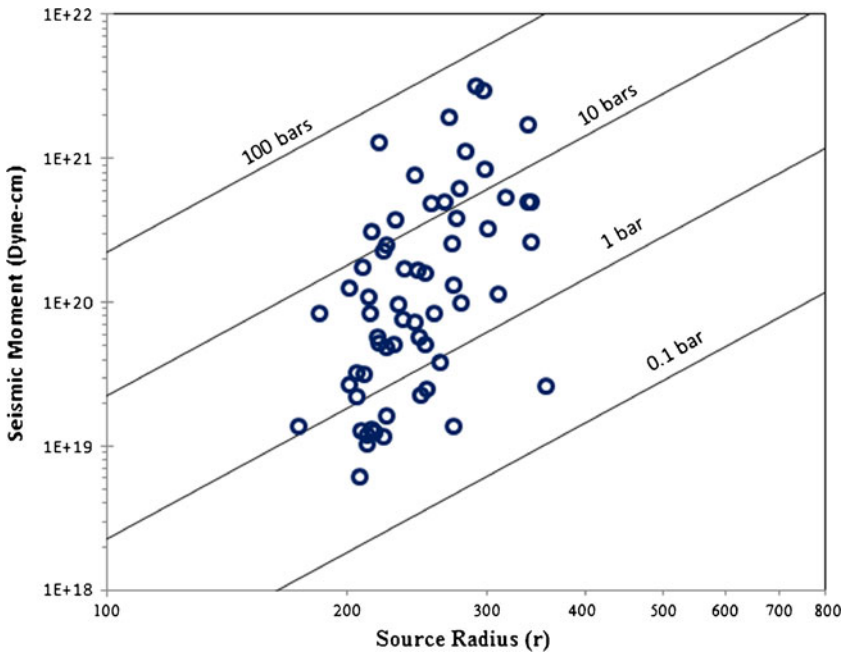

Fig. 4 Plot between source radius and seismic moment

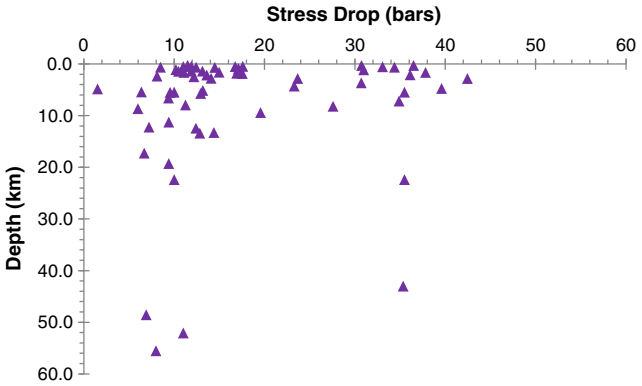

Fig. 5 Plot between stress drop and focal depth

The seismic moment is estimated from the value of Ω_0 following Kellis-Borok (1960) as:

$$\text{Seismic moment}, M_0 = \frac{4\pi\rho\beta^3 R\Omega_0}{R_{\theta\varphi}S_a} \quad (3)$$

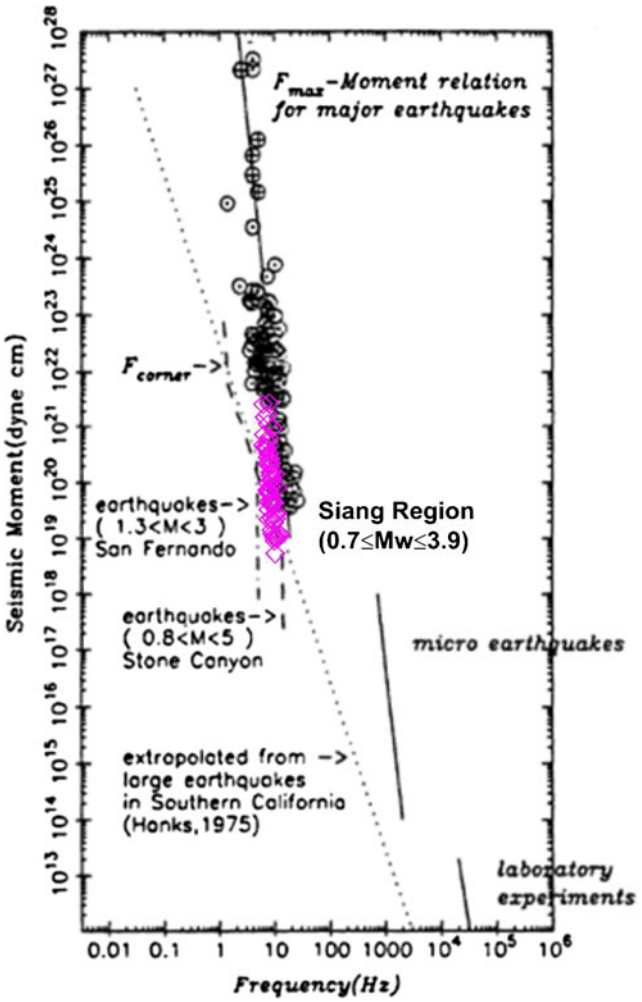

Fig. 6 Plot between f_{max} and seismic moment, M_0. The values of f_{max} obtained from Kameng (NE India) (*open diamonds*) are overlain on results of f_{max} from worldwide values complied by Aki (1988)

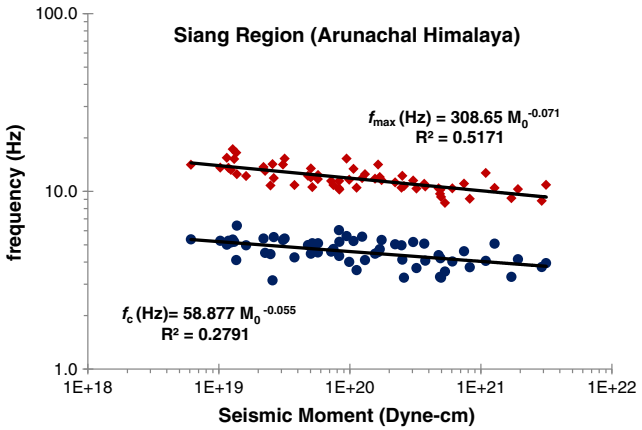

Fig. 7 Plot showing variation of average values of f_c and f_{max} with seismic moment for Siang Region of Arunachal Himalaya

Here, ρ is the average density(=2.67 g/cm^3), β is shear wave velocity in the source zone(=3.2 km/s), R is the hypocentral distance, $R\theta\varphi$ is the average radiation pattern (=0.63), Sa is free surface amplification(=2).

The moment magnitude has been estimated following Hanks and Kanamori (1979) as:

$$\text{Moment magnitude}, M_w = \frac{2}{3}\log M_0 - 10.73 \quad (4)$$

Following Brune (1970, 1971), source radius and stress drop are estimated as:

$$\text{Source radius}, r = \frac{2.34\beta}{2\pi f_c} \quad (5)$$

$$\text{Stress drop}, \Delta\sigma = \frac{7M_0}{16r^3} \quad (6)$$

Estimation of hypocenter parameters

The hypocenter parameters of 60 events recorded on digital seismographs have been estimated using Hypoinverse

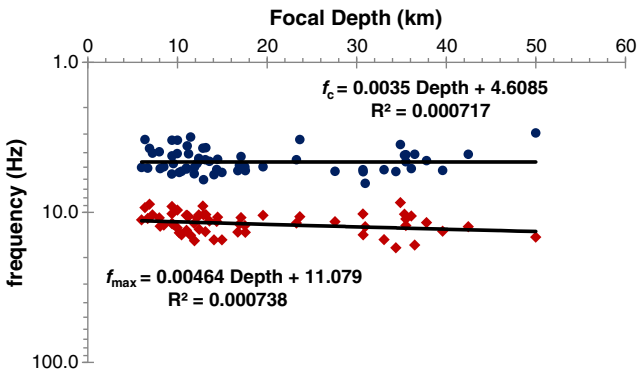

Fig. 8 Plot between focal depth and f_c and f_{max}

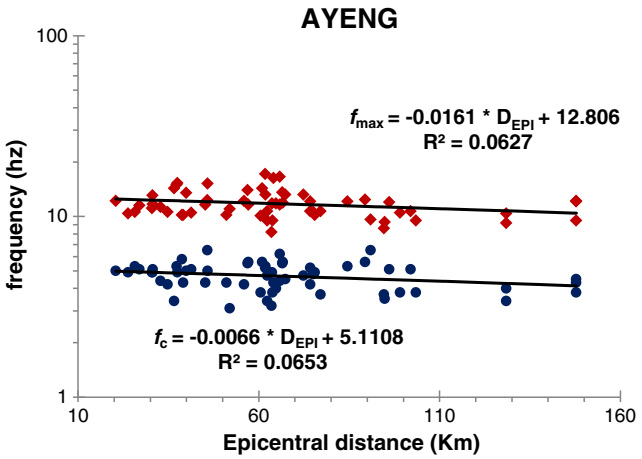

Fig. 9 Plot between epicentral distance (D_{EPI}) and f_c and f_{max}

program (Klein 1978) from their phase data. The velocity model in Table 1 for Shillong masiff given by Khattri et al. (1983) provided the best estimates of hypocenter parameters with minimum standard errors in the estimated parameters. Therefore, this velocity model has been adopted for estimating the hypocenter parameters. The standard errors in the estimation of hypocenter parameters for these events are ≤0.50 s in origin time (RMS), ≤5.0 km in epicenter (ERH) and≤5.0 km in focal depth (ERZ). These events approximately occur within hypocentral distances of about 120 km from various recording stations. All the 60 events were simultaneously recorded at three or more stations. Attempts have been made to estimate the hypocenter parameters of all the events simultaneously recorded at three or more stations. The epicenters of these events are plotted in Fig. 2.

Estimation of spectral and source parameters

A data set of 60 local events recorded on three component short-period and broad band seismometers with the sampling rate of 100 samples per second during July 2011 to February 2012 has been used to estimate the source parameters. The digital time series of local events have been corrected for baseline correction and for instrument response. For path correction, a frequency-dependent attenuation relation ($100f^{0.98}$), developed for the region from coda-waves of local earthquakes, has been applied (EQ: 2006-02). From the corrected source spectrum, the values of spectral parameters, viz. Ω_0, f_c and f_{max} were estimated using software EQK_SRC_PARA (Kumar et al. 2012), and the source parameters of the events have been estimated. A typical example of the time series of local earthquakes along with the estimated source spectra are depicted in Fig. 3 given below.

The estimated hypocenter parameters and source parameters, namely, seismic moment, source radius and stress drop for these events have been estimated and are listed in Table 2.

Results and discussions

Various plots have been prepared to study the characteristics of computed source parameters and the relationship among these parameters. These plots are discussed below:

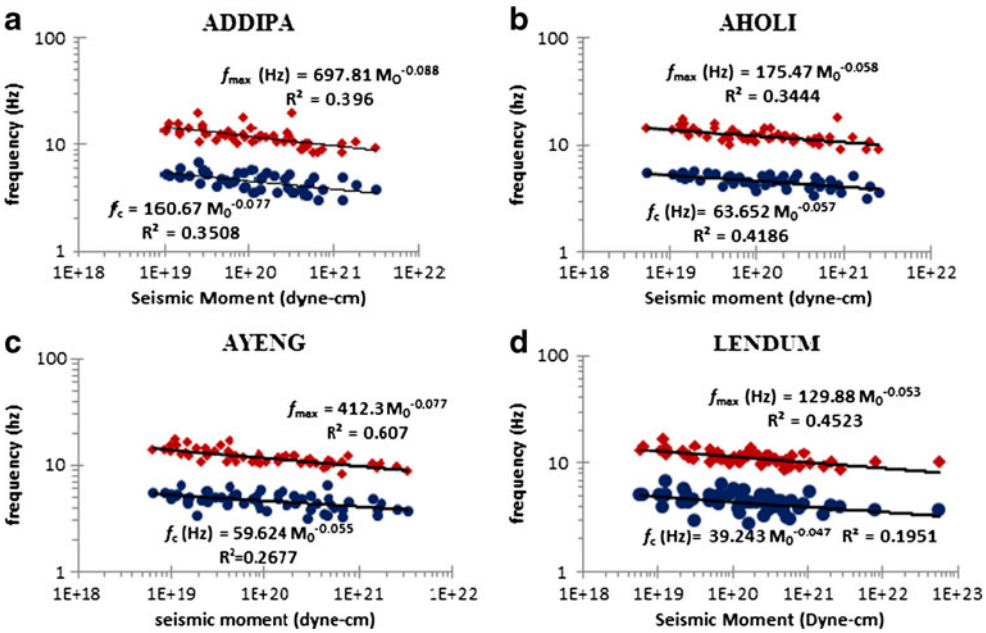

Fig. 10 Plot of f_c and f_{max} with seismic moment for **a** Addipa site, **b** Aholi site, **c** Ayeng site and **c** Lendum site

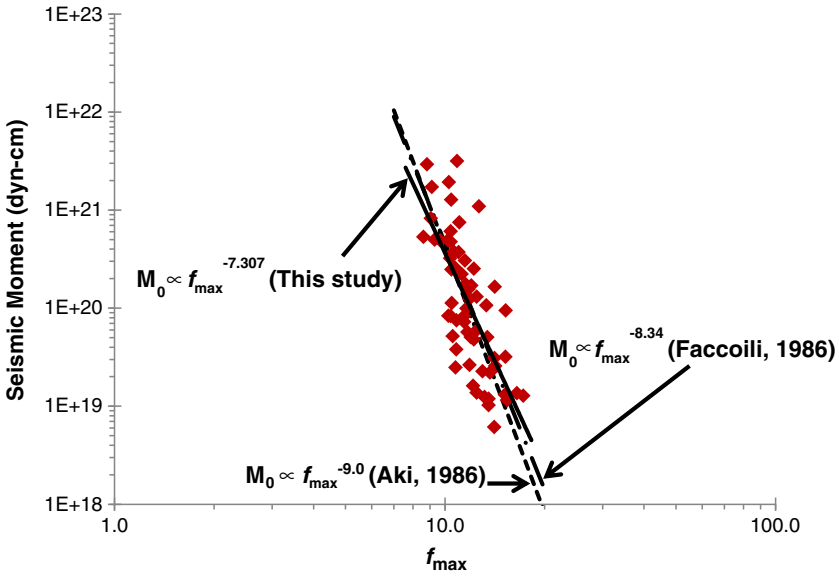

Fig. 11 Scaling laws proposed by Aki and Papageoriou (1988) (*dotted line*), Faccoili (1986) (*broken line*) and by this study (*solid line*) are shown in the figure

Source radius versus seismic moment Figure 4 shows the variation of source radius versus seismic moment for the 60 events. The linear curves corresponding to static stress drops of 0.1, 1 bar, 10 and 100 bars are also plotted. The source dimensions in terms of radius of the circular fault vary from about 175 to 357 m.

Stress drop The stress drops of these events vary from 0.2 to 56 bars and show large scatter (Fig. 3). Similar values of stress drops for microearthquakes have also been reported by other investigators (e.g. Archuleta et al. 1982; Dysart et al. 1988; Abercrombie1995; Garcia et al. 1996; Wu et al. 1999; Jin et al. 2000; Tusa and Gresta 2008; Kumar et al. 2006; Sule 2010; Kumar et al. 2012). The low value of stress drop might suggest that some microearthquake in this region should be associated with a britttle shear failure machenism on the fault segment and/or a presence of weakened zones where the earthquake may be triggered by low stress regimes.

Plot in Fig. 5 depicts the variation of stress drop with focal depth shows there is nothing any trend of stress drop with increasing focal depth.

f_{max}: It is a matter of active debate as to whether the f_{max} observed in the acceleration spectrum of an earthquake reflects the source characteristics or is on account of attenuation due to subsurface geological characteristics below the recording site (e.g. Hanks 1982; Papageorgiou and Aki 1983a; b; Campillo 1983; Anderson and Hough 1984; Anderson 1986, 1991; Morikawa and Sasatani 2000). The values of f_{max} and seismic moment, M_0, are plotted in Fig. 6 to allow comparison with the worldwide values of f_{max} complied by Aki (1988). The observed values of f_{max} agrees with worldwide observations.

Figure 7 showing the variations of f_c and f_{max} with seismic moment has been drawn to study the relationship to seismic source. Although the dataset shows large scatter, it seems from the plot that there is a similar decreasing trend for both f_c and f_{max} with increasing seismic moment or source size. Hence, it is concluded that f_{max} has similar dependence as f_c on seismic source.

Figures 8 and 9 depict plots of f_c and f_{max} to focal depth and epicentral distance. In both plots, a large scatter in data that follows a parallel trend to focal depth and epicentral distance has been observed, thus, dependence of f_{max} on focal depth and epicentral distance of earthquakes can also be excluded.

In order to study the dependence of f_{max} with the site characteristics, values of f_c and f_{max} are plotted between seismic moments for each site.

The plots shown in Fig. 10a, b, c and d indicate similar scatter and almost parallel trends for both f_c and f_{max} with increasing seismic moment. Thus, this indicates that f_{max} has similar behavior as f_c to seismic moment on each site that shows it is also due to source process and gets affected by site effects in a similar manner as f_c.

In a similar study by Tsai and Chen (2000), they fitted a regression model in terms of distance, earthquake magnitude and site and showed that the high-cut process is controlled by both the site and source effects. They also inferred that distance is the least significant parameter controlling the high-cut process. Similar results have been presented by Kumar et al. (2013a, b) for local events that occurred in the Kameng region of Arunachal Lesser Himalaya and Bilaspur region of Himachal Lesser Himalaya.

In the following, relationships of f_{max} with seismic moment and stress drop from the local earthquakes that occurred in this region have been obtained:

$$M_0(\text{dyne-cm}) = 7 \times 10^{27} {f_{max}}^{-7.307}$$

$$\Delta\sigma(\text{bars}) = 6 \times 10^{6} {f_{max}}^{-5.854}$$

Some of the researchers have reported the relationship between f_{max} and seismic moment as given below:

$\log f_{max} = -0.12 \log M_0 + 3.864$ (Faccioli 1986)

$\log f_{max} = -0.018 \log M_0 + 1.58$ (Satoh et al. 1997)

$\log \Delta\sigma = -2.91 \log M_0 + 5.8$ (Satoh et al. 2000)

Aki and Papageorgiou (1988) suggested the relationship $M_0 \propto {f_{max}}^{-9}$ from data in California, and Faccioli (1986) obtained relationship $M_0 \propto {f_{max}}^{-8.39}$ from data in Italy and Yugoslavia. In this study, a relationship, $M_0 \propto {f_{max}}^{-7.307}$ (Fig. 11) is obtained from local earthquakes data, and the difference may be due to the different environments or the earthquakes of small magnitudes studied.

Conclusions

For the Siang region that falls in the Arunachal Lesser Himalaya, source parameters and f_{max} of 60 local events have been estimated and interpreted. The 60 local events studied have moment magnitudes between 1.9 and 3.6. The source dimensions in terms of radius of the circular fault vary from about 175 to 357 m. The stress drops of these events vary from 0.2 to 56 bars. The variation of stress drop with focal depth shows no relation of stress drop with increasing focal depth.

The f_{max} estimated from these local earthquakes conforms to the worldwide observations made by Aki (1988). Dependence of f_{max} on source, depth of occurrence, epicentral distance and site has been studied on the basis of comparative dependency of f_c and f_{max}. The various plots of both f_c and f_{max} with seismic moment, depth, epicentral distance and site showed the same amount of scatters and trends. From this study, it is found that f_{max} has similar behavior as f_c to seismic moment that shows it is also due to source process and gets affected by site effects in a similar manner as f_c. Both f_c and f_{max} are found independent of epicentral distance and depth of occurrence. Similar results have been presented by Kumar et al. (2013a, b) for local events occurring in the Kameng region of Arunachal Lesser Himalaya and Bilaspur region of Himachal Lesser Himalaya.

Acknowledgments The authors are thankful to Ashwani Kumar, Hans Raj Wason and Ashok Kumar for their valuable guidance and support in carrying out this research work. The authors are also thankful to Jaypee Ventures Pvt. Ltd., Noida, for funding the project under which data were collected.

References

Abercrombie RE (1995) Earthquake source scaling relationships from 1 to 5 M_L using seismograms recorded at 2.5 km depth. J Geophys Res 100:24015–24036

Aki K (1967) Scaling law of seismic spectrum. J Geophys Res 72: 1217–1231

Aki K (1987) Magnitude–frequency relation for small earthquakes: a clue to the origin of f_{max} of large earthquakes. J Geophys Res 92:1349–1355

Aki K (1988) Physical theory of earthquakes. In: Bonnin, J., Cara, M., Cisternas, A., Fantechi, R. (eds.), Seismic Hazard in Mediterranean Region 3–33

Aki K, Papageorgiou AS (1988) Separation of source and site effects in acceleration power spectral of major California earthquakes. In Proc. 9th WCEE 8:163-167

Anderson JG (1986) Implication of attenuation for studies of the earthquake source. In: Das S, Boatwright J, Scholz CH (eds) Earthquake source mechanics, Maurice Ewing series 6. American Geophysical Union, Washington, D.C., pp 311–318

Anderson JG (1991) A preliminary descriptive model for the distance dependence of the spectral decay parameter in southern California. Bull Seismol Soc Am 81:2186–2193

Anderson JG, Hough SE (1984) A model for the shape of the Fourier amplitude spectrum of acceleration at high frequencies. Bull Seismol Soc Am 74:1969–1993

Archuleta RJ, Cranswick E, Mueller C, Spudich P (1982) Source parameters of the 1980 Mammoth Lakes, California, earthquake sequence. J Geophys Res Solid Earth 87(B6):4595–4607

Boore DM (1983) Stochastic simulation of high-frequency ground motion based on seismological models of the radiated spectra. Bull Seismol Soc Am 73:1865–1894

Brune JN (1970) Tectonic stress and the spectra of seismic shear waves from earthquake. J Geophys Res 75:4997–5009

Brune JN (1971) Correction to tectonic stress and the spectra of seismic shear waves from earthquakes. J Geophys Res 76:5002

Campillo M (1983) Numerical evaluation of near-field, high-frequency radiation from quasi-dynamic circular faults. Bull Seismol Soc Am 73:723–734

Dysart PS, Snoke JA, Sacks IS (1988) Source parameters and scaling relations for small earthquakes in the Matsushiro region, southwest Honshu, Japan. Bull Seismol Soc Am 78:571–589

EQ: 2006-02 Report on source parameters and attenuation characteristics in the environs of Bichom and Tenga dam sites, Kameng hydroelectric project, Arunachal Pradesh. Department of Earthquake Engineering, IIT Roorkee.

Faccioli E (1986) A study of spectra and peak values of strong motion accelerograms from Italy and Yugoslavia in terms of gross source properties, in Earthquake Source Mechanics, Geophysical Monograph 37, Maurice Ewing Series, vol. 6, S. Das, J. Boatwright, and C. H. Scholz, Editors, American Geophysical Union, Washington, D.C., pp 297-310

Fujiwara H, Irikura K (1991) High-frequency seismic wave radiation from antiplane cohesive zone model and f_{max} as source effect. Bull Seismol Soc Am 81(4):1115–1128

Gansser A (1964) Geology of the Himalaya. Interscience Publications, London, pp 1–273

García-García JM, Vidal F, Romacho MD, Martín-Marfil JM, Posada A, Luzón F (1996) Seismic source parameters for microearthquakes of the Granada basin (southern Spain). Tectonophysics 261:51–66

GSI (2000) Seismotectonic Atlas of India and its environs. Geol. Surv. India, Sp. Pub., P. L. Narula, S. K. Acharya and J. Banerjee (eds.).

Hanks TC (1982) f_{max}. Bull Seismol Soc Am 72:1867–1879

Hanks TC, Kanamori H (1979) A moment magnitude scale. J Geophys Res 84:2348–2350

Jin A, Moya CA, Ando M (2000) Simultaneous determination of site responses and source parameters of small earthquakes along the Atotsugawa fault zone, central Japan. Bull Seismol Soc Am 90: 1430–1445

Kayal JR (1987) Microseismicity and source mechanism study: Shillong Plateau, Northeast India. Bull Seismol Soc Am 77:184–194

Keilis-Borok VI (1960) Investigation of the mechanism of earthquakes. Sov Res Geophys (English transl) 4:29

Khattri KN, Wyss M, Gaur VK, Saha SN, Bansal BK (1983) Local seismic activity in the region of the Assam gap, northeast India. Bull Seism Soc Am 73:459–469

Kinoshita S (1992) Local characteristics of the f_{max} of bedrock motion in the Tokyo metropolitan area, Japan. J Phys 40:487–515

Klein FW (1978) Hypocenter location program: HYPOINVERSE, U.S. Geol. Surv. Open-File Rep. 78-694, pp 113

Kumar G (1997) Geology of Arunachal Pradesh. Geological Society of India, Bangalore

Kumar A, Gupta SC, Kumar A, Sen A, Jindal AK, Jain S (2006) Estimation of source parameters from local earthquakes in Western part of the Arunachal Lesser Himalaya. In: 13th Symposium on Earthquake Engineering, pp 9–17

Kumar A, Kumar A, Mittal H, Kumar A, Bhardwaj R (2012) Software to estimate earthquake spectral and source parameters. Int J Geosci 3(5):1142–1149

Kumar A, Kumar A, Gupta SC, Mittal H, Kumar R (2013a) Source parameters and f_{max} in Kameng region of Arunachal Lesser Himalaya. J Asian Earth Sci 70–71:35–44

Kumar A, Kumar A, Gupta SC, Jindal AK, Ghangas V (2013b) Seismicity and source parameters of local earthquakes in Bilaspur region of Himachal Lesser Himalaya. Arabian J Geosci http://dx.doi.org/10.1007/s12517-013-0929-y

Le Fort P (1975) Himalaya, the collided range: present knowledge of the continental arc. American J Sci 275a:1-44

Morikawa N, Sasatani T (2000) The 1994 Hokkaido Toho-oki earthquake sequence: the complex activity of intra-slab and plate-boundary earthquakes. Phys Earth Planet Inter 121(1):39–58

Mukhopadhyay M (1984) Seismotectonics of transverse lineaments in the eastern Himalaya and foredeep. Tectonophysics 109:227–240

Nandy DR (1976) The Assam syntaxis of the Himalayas—a re-evaluation. Semin Rec Geol Study Himal Misc Publ Geol Surv India 24:363-368

Papageorgiou AS (1988) On two characteristic frequencies of acceleration spectra: patch corner frequency and f_{max}. Bull Seismol Soc Am 78:509–529

Papageorgiou AS, Aki K (1983a) A specific barrier model for the quantitative description of inhomogeneous faulting and the prediction of strong ground motion, part I: description of the model. Bull Seismol Soc Am 73:693–722

Papageorgiou AS, Aki K (1983b) A specific barrier model for the quantitative description of inhomogeneous faulting and the prediction of strong ground motion, part II: applications of the model. Bull Seismol Soc Am 73:953–978

Purvance MD, Anderson JG (2003) A comprehensive study of the observed spectral decay in strong-motion accelerations recorded in Guerrero, Mexico. Bull Seismol Soc Am 93:600–611

Satoh T, Kobayashi Y, Kawano H (2000) Stress drop and f_{max} from strong motion records observed at deep borehole in Japan. Proc. of the Twelfth World Conference on Earthquake Engineering, Auckland, New Zealand, 30 January–4 February

Satoh T, Kawase H, Sato T (1997) Statistical spectral model of earthquakes in the Eastern Tohoku District, Japan, based on the surface and borehole records observed in Sendai. Bull Seismol Soc Am 87(2):446–462

Singh S, Chowdhary PK (1990) An outline of the geological framework of the Arunachal Himalaya. J Himal Geol 1(2):189–197

Sule B (2010) Spectral source parameters for weak local earthquakes in the Pannonian basin. Cent Eur J Geosci 2(4):475–480

Tsai C-CP, Chen KC (2000) A model for the high-cut process of strong-motion accelerations in terms of distance, magnitude, and site condition: an example from the SMART 1 array, Lotung, Taiwan. Bull Seismol Soc Am 90(6):1535–1542

Tsurugi M, Tai M, Kowada A, Tatsumi Y, Irikura K (2000) Estimation of empirical site amplification effects using observed records. 12 WCEE 1243:1-6

Tsurugi M, Kagawa T, Irikura K (2008) Study on high-cut frequency characteristics of ground motions for inland crustal earthquakes in Japan. WCEE 14:02–0036

Tusa G, Gresta S (2008) Frequency-dependent attenuation of P waves and estimation of earthquake source parameters in southeastern Sicily, Italy. Bull Seismol Soc Am 98:2772–2794

Verma RK, Mukhopadhyay M, Ahluwalia MS (1976) Seismicity, gravity and tectonics of Northeast India and Northern Burma. Bull Seismol Soc Am 66:1683–1694

Wen J, Chen X (2012) Variations in f_{max} along the ruptured fault during the M_w 7.9 Wenchaun earthquake of 12 may 2008. Bull Seismol Soc Am 102(3):991–998

Wu ZL, Chen YT, Mozaffari P (1999) Scaling of stress drop and high-frequency fall-off of source spectra. Acta Seismol Sin 12(5):507–515

Yokoi T, Irikura K (1991) Meaning of source controlled f_{max} in empirical Green's function technique based on a T^2-scaling law. Annuals of Disaster Prevention Research Institute, Kyoto University 34 B-1: 177–189